Impact of nutritional factors on in vitro PK/PD modelling of polymyxin B against various strains of Acinetobacter baumannii

Mathilde Lacroix, Jérémy Moreau, Claudia Zampaloni, Caterina Bissantz, Hamasseh Shirvani, Sandrine Marchand, William Couet, Alexia Chauzy

International Journal of Antimicrobial Agents 64 (2024) 107189

Contents lists available at ScienceDirect

International Journal of Antimicrobial Agents

journal homepage: www.elsevier.com/locate/ijantimicag

Impact of nutritional factors on *in vitro* PK/PD modelling of polymyxin B against various strains of *Acinetobacter baumannii*

Mathilde Lacroix[a,b], Jérémy Moreau[a], Claudia Zampaloni[c], Caterina Bissantz[d], Hamasseh Shirvani[b], Sandrine Marchand[a,e], William Couet[a,e], Alexia Chauzy[a,*]

[a] *Université de Poitiers, INSERM U1070, PHAR2, Poitiers, France*
[b] *Institut Roche, Boulogne-Billancourt, France*
[c] *Roche Pharma Research and Early Development, Immunology, Infectious Disease and Ophthalmology, Roche Innovation Centre Basel, F. Hoffmann-La Roche Ltd, Basel, Switzerland*
[d] *Roche Pharma Research and Early Development, Pharmaceutical Sciences, Roche Innovation Centre Basel, F. Hoffmann-La Roche Ltd, Basel, Switzerland*
[e] *Département de Pharmacocinétique et Toxicologie, CHU Poitiers, Poitiers, France*

ARTICLE INFO

Article history:
Received 29 September 2023
Accepted 25 April 2024

Editor: Dr Y-W Lin

Keywords:
A. baumannii
Polymyxin B
PK/PD modelling
Cations
CAMHB dilution effect

ABSTRACT

The main objective of this study was to assess the effect of rich artificial cation-adjusted Mueller-Hinton broth (CAMHB) on the growth of three strains of *Acinetobacter baumannii* (ATCC 19606 and two clinical strains), either susceptible or resistant to polymyxin B (PMB), and on PMB bactericidal activity. A pharmacokinetic (PK)/pharmacodynamic (PD) modelling approach was used to characterize the effect of PMB in various conditions.

Time-kill experiments were performed using undiluted CAMHB or CAMHB diluted to 50%, 25% and 10%, with or without Ca^{2+} and Mg^{2+} compensation (known to affect PMB activity), and with PMB concentrations ranging from 0.25 to 256 mg/L based on the strain's MIC. For each strain, time-kill replicates were modelled using NONMEM.

Unexpectedly, dilution of CAMHB by up to 10-fold did not affect the growth rate of any of the three strains in the absence of PMB. However, the bactericidal activity of PMB increased with medium dilution, resulting in a reduction in the apparent bacterial regrowth of the various strains observed after a few hours. Data for each strain were well characterized by a PK/PD model, with two bacterial subpopulations with different susceptibility to PMB (more susceptible and less susceptible). The impact of medium dilution and cation compensation showed relatively high, unexplained between-strain variability. Further studies are needed to characterize the mechanism underlying the medium dilution effect.

1. Introduction

The optimization of antibiotic dosing regimens often relies on pharmacokinetic/ pharmacodynamic (PK/PD) indices, such as maximal unbound drug concentration over minimum inhibitory concentration (*f*Cmax/MIC), percentage of time period that the drug concentration is above the MIC (%*f*T>MIC), and area under the unbound drug concentration–time curve over MIC (*f*AUC/MIC). However, these indices suffer from several limitations [1], and more sophisticated approaches to capture the complexity of antibiotic–bacteria interactions, such as semi-mechanistic or mechanistic PK/PD modelling [2], have been reported increasingly in the literature [3].

However, although these new approaches are highly interesting, they are often based on *in vitro* experiments such as time-kill (TK) experiments or the Hollow Fiber Infection Model (HFIM), which may not translate directly to *in vivo*. Indeed, linking *in vitro* PD models with in-vivo PK to predict in-vivo outcomes via Monte Carlo simulations has been reported, but a lack of correlation between bacterial count vs. time profiles predicted by *in vitro* PD models and those actually observed *in vivo* in neutropenic rodents has been described on several occasions [4–9]. To predict in-vivo data from *in vitro* PD models combined with in-vivo PK, some model parameters related to antibiotic activity [7], or to both antibiotic activity and bacterial growth [4–6], or even model structure [8,9] had to be refined. There are several reasons for the lack

* Corresponding author. Address: INSERMU1070, Université de Poitiers, Pôle Biologie Santé, Bâtiment B36, 1 rue Georges Bonnet, 86022 Poitiers Cedex, France.
E-mail address: alexia.chauzy@univ-poitiers.fr (A. Chauzy).

https://doi.org/10.1016/j.ijantimicag.2024.107189

of correlation between *in vitro* and in-vivo data, including specific in-vivo aspects such as host defences or the presence of biofilm; these are not usually taken into account *in vitro*, with a few exceptions [10,11]. On the other hand, among the various causes of discrepancy between *in vitro* and in-vivo PD, the composition of the culture media used *in vitro* could play a significant role by not reflecting the environment of the bacteria at the infection site. Bacteria evolve in different and complex micro-environments, where nutrient availability can differ with pathophysiological conditions, as inflammation is known to increase the carbon source, amino acids, vitamins and iron at the action site [12] or between different infection sites. For example, bacteria responsible for intracellular infections have access to an important source of nutrients [13], as do those in lung infections where biofilms are present [14], whereas nutrients are less abundant in cerebrospinal fluid (CSF) infections [15] and urinary tract infections [16]. Although culture media are occasionally selected to mimic body fluids such as CSF [17] or peritoneal fluid [18], rich artificial media are often used due to their ability to promote bacterial growth; these media do not necessarily reflect in-vivo conditions, where the bacterial growth rate has been found to be higher *in vitro* compared with *in vivo* [5,19]. Among *in vitro* culture media, cation-adjusted Mueller-Hinton broth (CAMHB) has been used preferentially for years, and is recognized nowadays as a standard by the Clinical and Laboratory Standards Institute (CLSI) and the European Committee on Antimicrobial Susceptibility Testing (EUCAST) [20,21]. A previous study investigated the effect of nutrient concentration via CAMHB dilutions on the growth of *Pseudomonas aeruginosa* ATCC 27853 and the antimicrobial activity of meropenem [22]. The results showed a decrease in bacterial growth rate, an increase in kill rate, and a decrease in meropenem MIC with medium dilution. In addition to nutrients, cations present in CAMHB could affect the activity of antibiotics such as polymyxins by displacing them from binding to lipopolysaccharides on the outer membrane of bacteria [23].

The aim of this study was to investigate the effect of nutrient concentration and cations present in CAMHB on another bacteria/antibiotic pair – *Acinetobacter baumannii*/polymyxin B (PMB) – for which discrepancies between *in vitro* and *in vivo* have been observed previously [9], using a PK/PD modelling approach distinguishing the medium effect on bacterial growth, the initial decrease in colony-forming unit (CFU) count, and apparent regrowth.

2. Materials and methods

2.1. Chemical and strains

PMB was obtained from Sigma-Aldrich (Saint-Quentin Fallavier, France), and used to prepare stock solutions of 10 mg/mL in sterile water. *A. baumannii* ATCC 19606 and two clinical multi-drug-resistant strains of *A. baumannii*, isolated from a patient before (AB121-D0) and 12 days after treatment with colistin (AB122-D12) [24], were used in this study. AB121-D0 was susceptible to PMB, while AB122-D12 became resistant.

2.2. MIC determination

The MICs of the three *A. baumannii* strains were determined in duplicate, at least, by micro-dilution in accordance with the EUCAST and CLSI recommendations [20,21] in commercial cation-adjusted Mueller-Hinton broth II (CAMHB-100%) (bioMérieux, Marcy-l'Etoile, France) or diluted in water at 1:2 (CAMHB-50%), 1:4 (CAMHB-25%) or 1:10 (CAMHB-10%) with or without cation compensation to reach the CAMHB-100% level.

2.3. Time-kill experiments with various dilutions of CAMHB

The three strains were cultured overnight in CAMHB-100% with shaking (150–170 rpm) at 35°C. These cultures were diluted to 1/50 in CAMHB-100%, and incubated at 35°C with shaking until an optical density of 0.3 (corresponding to 1.10^8 CFU/mL of bacteria in exponential growth phase) was achieved. The bacterial precultures were diluted to obtain a starting inoculum at 10^6 CFU/mL in CAMHB-100% or diluted at 50%, 25% and 10%. TK experiments were performed with various PMB concentrations, including MIC values, ranging from 0.125 to 256 mg/L. Drug-free CAMHB was used as a bacterial growth control for each CAMHB dilution and strain. These cultures were incubated at 35°C, and bacterial samples were collected over time at 0, 1, 3, 6, 10, 24 and 30 h. Samples were serially diluted in NaCl 0.9% and plated on to Mueller-Hinton agar supplemented with 1% activated charcoal (to prevent PMB carry-over effect [25,26]). Bacteria were counted after overnight incubation at 35°C. The limit of quantification was 400 CFU/mL (i.e. 2.6 $\log_{10}$ CFU/mL). Experiments were conducted in triplicate for the three *A. baumannii* strains and each CAMHB dilution.

2.4. Time-kill experiments with CAMHB dilution and cation compensation

Additional TK experiments were performed in triplicate with the three *A. baumannii* strains, following the same protocol as described above but with cation (Ca^{2+} and Mg^{2+}) compensation in diluted CAMHB in order to restore the concentrations found in CAMHB-100% (i.e. 20 mg/L of calcium and 10 mg/L of magnesium) [27]. PMB concentrations ranged between 0.25 and 64 mg/L depending on the strain's MIC.

2.5. Pharmacodynamic model

Bacterial counts obtained from TK experiments without cation compensation were modelled using NONMEM 7.4 (ICON plc, Dublin, Ireland), with the Laplacian algorithm and the M3 method for handling observations below the limit of quantification [28]. For each strain, TK replicates obtained for all CAMHB dilutions (without cation compensation) were modelled simultaneously. As shown previously [29] and after a quick experimental check of the stability of PMB (10 mg/L) in CAMHB and water at 35°C for 96 h (not shown), PMB was assumed to be stable over the course of the experiment. A previously described PD model with heteroresistance [30] [i.e. two bacterial sub-populations differing in drug susceptibility, with S^+ representing the more susceptible (and the vast majority of) bacteria at 0 h, and S^- representing the less susceptible bacteria developing progressively over time] was used to describe the time course of bacterial counts (CFU/mL) for the three *A. baumannii* strains (Fig. 1). Briefly, a logistic growth model with one compartment for each bacterial sub-population was used to describe self-limited bacterial growth in the absence of antibiotic (Eqs. 1 and 2):

$$\frac{dS^+}{dt} = k_{net} \times \left(1 - \frac{S^+ + S^-}{BMAX}\right) \times S^+ \quad (1)$$

$$\frac{dS^-}{dt} = k_{net} \times \left(1 - \frac{S^+ + S^-}{BMAX}\right) \times S^- \quad (2)$$

where k_{net} (/h) is the apparent growth rate constant, and BMAX (CFU/mL) is the maximal capacity of the system.

The effect of PMB on bacterial killing (kill rate) was characterized by a sigmoidal Emax model (Eq. 3), where Emax (/h) represents the maximum kill rate, EC_{50} (mg/L) represents the concentration of PMB needed to reach 50% of the maximum effect, C (mg/L) represents the concentration of PMB, and γ represents the

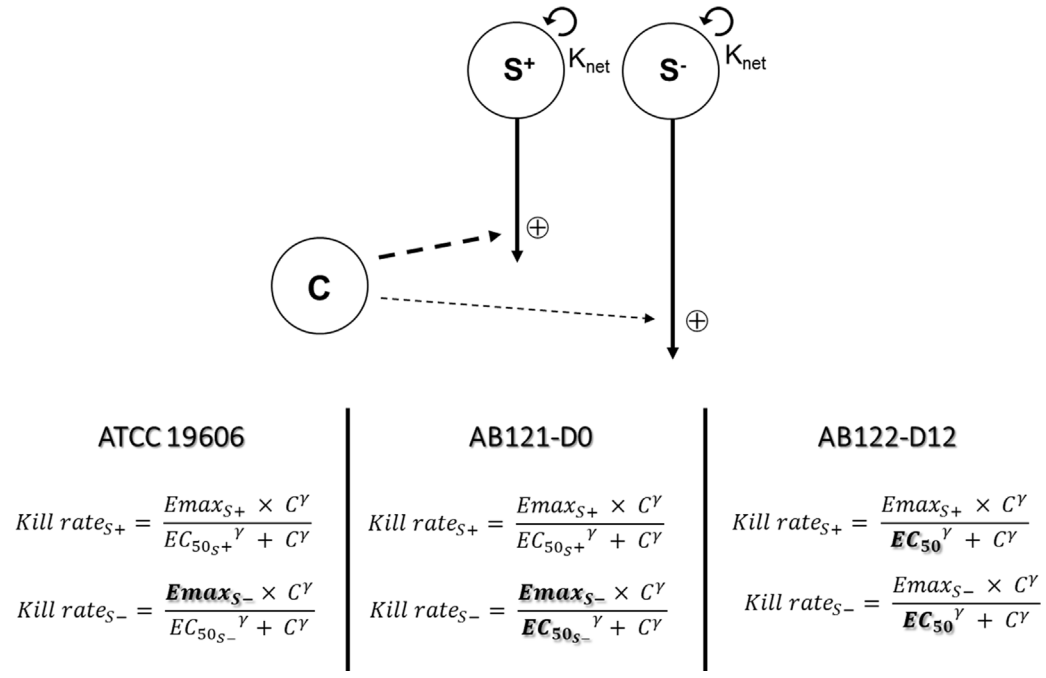

Fig. 1. Pharmacokinetic/pharmacodynamic model structure for the three strains. K_{net}, apparent growth rate constant (/h); S^+, more susceptible bacterial sub-population; S^-, less susceptible bacterial sub-population; C, polymyxin B concentration (mg/L); Emax, maximum kill-rate constant due to polymyxin B (PMB) (/h); EC_{50}, PMB concentration needed to reach 50% of Emax (mg/L); γ, Hill coefficient. Medium dilution affected $Emax_{S-}$ for ATCC 19606, $Emax_{S-}$ and $EC_{50,S-}$ for AB121-D0, and EC_{50} common to both bacterial subpopulations for AB121-D12.

Hill coefficient. PMB affected both sub-populations, but differences in Emax, EC_{50} or both were tested to characterize the difference in PMB susceptibility between S^+ and S^-. The PMB kill rate was incorporated into Eqs. 1 and 2, as described in Eqs. 4 and 5:

$$Kill\ rate = \frac{Emax \times C^{\gamma}}{EC_{50}{}^{\gamma} + C^{\gamma}} \quad (3)$$

$$\frac{dS^+}{dt} = k_{net} \times \left(1 - \frac{S^+ + S^-}{BMAX}\right) \times S^+ - Kill\ rate_{S+} \times S^+ \quad (4)$$

$$\frac{dS^-}{dt} = k_{net} \times \left(1 - \frac{S^+ + S^-}{BMAX}\right) \times S^- - Kill\ rate_{S-} \times S^- \quad (5)$$

where kill $rate_{S+}$ and kill $rate_{S-}$ (/h) are the kill rates of S^+ and S^- respectively.

For each strain, the impacts of CAMHB dilution on the bacterial growth rate and killing rate due to PMB were investigated by estimating separate parameters for each dilution. Parameters affected by CAMHB dilution were then re-estimated using TK data obtained with cation compensation, while keeping the other parameters fixed. In the final model, parameters for TK data with and without cation compensation were estimated simultaneously.

Model selection was based on objective function value, relative standard error of the parameter estimates obtained using the sampling importance resampling procedure implemented in Perl-speaks-NONMEM [31], and goodness-of-fit (GOF) plots. Visual predictive checks with stratification for PMB concentration, CAMHB dilution and cation compensation were drawn to evaluate the predictive performance of the model, and taken into account for model selection. Observed bacterial counts were plotted vs. time, and overlaid with the median and 90% prediction interval obtained by simulating 1000 replicates of the original data set. The concordance between simulations and observations was inspected visually.

2.6. Simulation of bacterial killing rate at different PMB concentrations

Simulations of expected PMB kill rate (Eq. 3) for both S^+ and S^- sub-populations at constant PMB concentrations ranging from 0 to 1000 mg/L were performed using R Version 4.1.3 to compare the impact of CAMHB dilution with and without cation compensation between the three *A. baumannii* strains.

3. Results

3.1. Medium effect on MIC

Using CAMHB-100%, PMB MIC was estimated at 0.25 mg/L for ATCC 19606 and 0.5 mg/L for AB121-D0, and the effect of CAMHB dilution without or with cation compensation was minor (Table 1). For AB122-D12, the MIC was assessed at 128 mg/L in CAMHB-100%, with a major reduction after medium dilution (MIC = 2 mg/L in CAMHB-10%) as shown in Table 1. Cation compensation decreased the MIC reduction observed with medium dilution (MIC = 32 mg/L in CAMHB-10% with cation compensation).

3.2. Time-kill results with CAMHB dilution

No dilution effect on apparent bacterial growth was observed in the absence of antibiotic for the three *A. baumannii* strains [Fig. S1 (first column), see online supplementary material].

For ATCC 19606, regrowth was observed after an initial CFU decay for PMB concentrations up to 16 mg/L, corresponding to 64-fold the MIC in CAMHB-100% (Fig. S1A, see online supplementary material). CAMHB dilution had a minimal impact for PMB concentrations below and around the MIC, but above the MIC, bacterial regrowth became less apparent with dilution. The highest PMB concentration for which regrowth was observed decreased from 16 mg/L in CAMHB-100% to 1 mg/L in CAMHB-10%.

Table 1
Minimum inhibitory concentration (MIC) values in diluted cation-adjusted Mueller-Hinton broth (CAMHB) with (w/) and without (w/o) cation compensation

MIC (mg/L)	ATCC 19606		AB121-D0		AB122-D12	
	w/	w/o	w/	w/o	w/	w/o
CAMHB-100%	0.25		0.5		128	
CAMHB-50%	0.5	0.25	0.5	0.5	128	64
CAMHB-25%	0.5	0.5	1	1	64	16
CAMHB-10%	1	1	2	2	32	2

For AB121-D0, comparable results to ATCC 19606 were observed (Fig. S1B, see online supplementary material). The highest PMB concentration for which regrowth was observed decreased from 16 mg/L in CAMHB-100% to 2 mg/L in CAMHB-10%.

For AB122-D12, bacterial regrowth was observed for concentrations up to 128 mg/L in CAMHB-100% and in the presence of PMB (Fig. S1C, see online supplementary material). However, CAMHB dilution had a more pronounced effect on this strain, with a 64-fold reduction in the highest concentration showing regrowth between CAMHB-100% and CAMHB-10% (128 vs. 2 mg/L).

For all strains, most variability between experiments was observed at concentrations of 0.5–2 x MIC.

3.3. Time-kill experiments with CAMHB dilution and cation compensation

For ATCC 19606, TK experiments performed with cation compensation in diluted medium conditions (50%, 25% and 10%) revealed similar results compared with the data obtained without cation compensation (Fig. S2A, see online supplementary material).

For AB121-D0, when cations were compensated, comparable results were obtained for CAMHB-50%, CAMHB-25% and CAMHB-10%, suppressing the medium dilution effect. These combined results were similar to CAMHB-100% despite important variability between replicates (Fig. S2B, see online supplementary material).

For AB122-D12, cation compensation reduced the medium dilution effect but did not restore the CAMHB-100% results. For the same concentration of PMB, a greater decrease in CFU count was observed in diluted medium with cation compensation compared with CAMHB-100% (Fig. S2-C, see online supplementary material).

3.4. PK/PD modelling of the medium dilution effect

The selected PK/PD models gave a good description of the TK data, as shown in the GOF plots available in Fig. S3 (see online supplementary material) and the visual predictive checks in Figs. 2 and S4 (see online supplementary material). For ATCC 19606 and AB121-D0, the PMB effect parameters Emax and EC_{50} differed for each bacterial sub-population, while only Emax differed between the sub-populations for AB122-D12 (Fig. 1).

3.4.1. Effect of CAMHB dilution on model parameters

For all three *A. baumannii* strains, bacteria-specific parameters (i.e. k_{net} and BMAX) were not affected by medium dilution, unlike the model parameters characterizing the bactericidal effect of PMB.

For ATCC 19606, the dilution effect was observed solely for the S^- sub-population. CAMHB dilution had a moderate impact on $Emax_{S-}$, with a 2.15-fold increase between CAMHB-100% and CAMHB-10% (Table S1A and Fig. S5, see online supplementary material). For this strain, similar $Emax_{S-}$ values were estimated for TK experiments with and without cation compensation, except for CAMHB-50% which exhibited a modest (1.15-fold) increase between data with and without cation compensation.

For AB121-D0, a dilution effect was observed solely for the S^- sub-population, as for ATCC 19606. However, in addition to an effect on $Emax_{S-}$, CAMHB dilution also impacted $EC_{50,S-}$, for which a 3.8-fold increase was observed between CAMHB-100% and CAMHB-10% (Table S1B and Fig. S5, see online supplementary material). With cation compensation, $EC_{50,S-}$ still increased with medium dilution ($EC_{50,S-}$ in CAMHB-10% with cations ~5-fold the value in CAMHB-100%), whereas $Emax_{S-}$ remained similar to CAMHB-100% (less than 13% differences between values).

For AB122-D12, the CAMHB dilution effect was characterized in both S^+ and S^- sub-populations by a 98% decrease in EC_{50} between CAMHB-100% and CAMHB-10%, this parameter being common to both S^+ and S^- sub-populations (60.4 and 1.13 mg/L for CAMHB-100% and CAMHB-10%, respectively) (Table S1C and Fig. S5, see online supplementary material). No additional medium effect on $Emax_{S-}$ was noted, unlike ATCC 19606 and AB121-D0, or $Emax_{S+}$. After cation compensation, EC_{50} decreased with medium dilution but to a lesser extent (EC_{50} in CAMHB-100% 60.4 mg/L, in CAMHB-10% with cation compensation 7.2 mg/L, in CAMHB-10% without cation compensation 1.13 mg/L).

3.4.2. Dilution effect on PMB kill rate

Simulations of the expected kill rates for various PMB concentrations and different CAMHB dilutions with and without cation compensation are shown in Figs. 3, 4 and S6 (see online supplementary material).

For ATCC 19606, for the S^+ sub-population, the kill rate increased with PMB concentration before reaching a plateau at 12.1/h, and was not impacted by CAMHB dilution. For the S^- sub-population, the kill rate increased with PMB concentration and also with CAMHB dilution. The plateau value also increased with CAMHB dilution, and reached $Emax_{S-}$ values of 1.61 and 3.79/h for CAMHB-100% and CAMHB-10%, respectively. Cation compensation did not impact kill-rate values (Figs. 4 and S6, see online supplementary material).

For AB121-D0, the kill rate increased with PMB concentration until plateauing, and the S^- sub-population alone was impacted by CAMHB dilution. However, for this strain, the dilution impact on kill $rate_{S-}$ varied with PMB concentration (Fig. 3). For PMB concentrations below approximately 3 mg/L, PMB kill rates were higher in CAMHB-100% and CAMHB-50% compared with CAMHB-25% and CAMHB-10% (e.g. at PMB 1 mg/L, kill $rate_{100\%}$ ~1.40/h and kill $rate_{10\%}$ ~1.08/h) (Figs. 4 and S6, see online supplementary material). However, above 3 mg/L, kill $rate_{S-}$ was higher in diluted medium, with plateau values equivalent to 1.87 and 3.04/h for CAMHB-100% and CAMHB-10% respectively. With cation compensation, maximum kill-$rate_{S-}$ values were reduced (at 10 mg/L, values for CAMHB-50%, CAMHB-25% and CAMHB-10% were reduced by approximately 38%, 21% and 20%, respectively, compared with values without cation compensation), and kill-$rate_{S-}$ values for CAMHB-50%, CAMHB-25% and CAMHB-10% had values similar to CAMHB-100% (Figs. 4 and S6, see online supplementary material).

For AB122-D12, kill rates for both S^+ and S^- sub-populations were impacted by medium dilution, and followed sigmoidal profiles (Fig. 3). For the S^+ sub-population, medium dilution did not modify the maximum value (equivalent to 21.90/h), but decreased the concentration needed to reach it, which translated to a shift

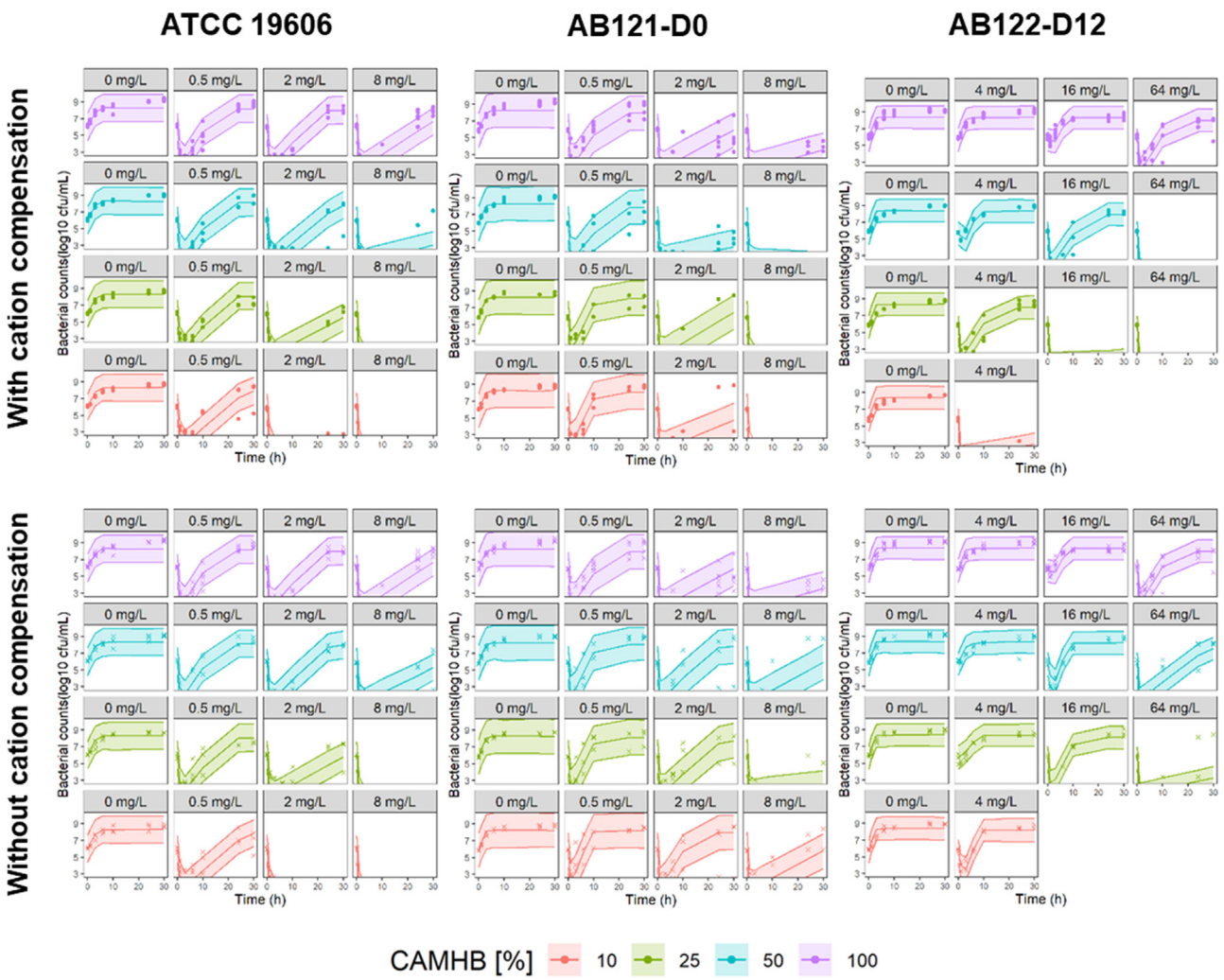

Fig. 2. Visual predictive checks for the final model. Circles (top panels) represent experimental time-kill data obtained in undiluted (purple) or 50% (blue), 25% (green) and 10% (red) diluted cation-adjusted Mueller-Hinton broth (CAMHB) without cation (Ca^{2+} and Mg^{2+}) compensation, and crosses (bottom panels) represent those obtained in diluted CAMHB with cation compensation. The coloured areas depict the 90% prediction interval based on 1000 simulations under the final model for a selection of tested concentrations of polymyxin B. Solid lines represent the 5th, 50th and 95th percentiles of those simulations.

to the left related to the degree of CAMHB dilution, corresponding to the decrease in EC_{50} between CAMHB-100% and CAMHB-10% (Table S1, see online supplementary material). Similar results were observed for the S^- sub-population with a maximum kill-rate value of 2.99/h. When cations were compensated in the medium, the observed shift to the left of the kill-rate curves for both the S^+ and S^- sub-populations was reduced (Figs. 4 and S6, see online supplementary material).

4. Discussion

Although artificial *in vitro* culture media have been developed to promote bacterial growth, this study found that dilution of CAMHB by up to 10-fold did not affect the growth rate of the three studied strains of *A. baumannii* in the absence of antibiotic, confirming previous results for this species [32]. Another study found that medium dilution led to an increase in the initial reduction in *P. aeruginosa* CFU count with time in the presence of meropenem, and regrowth was observed but not characterized [22]. However, in the present study, the initial CFU decrease with time was too rapid for precise characterization and assessment of the medium dilution effect, except for AB122-D12. On the other hand medium dilution reduced the apparent bacterial regrowth of the various strains progressively. For ATCC 19606 and AB121-D0, no medium dilution effect was observed for the S^+ sub-population, and only a modest impact on the kill rate was observed for the S^- sub-population, with an increase of less than a factor of 2 between the values at CAMHB-100% and CAMHB-10% (Fig. 2). In contrast, for AB122-D12, the kill rates for both the S^+ and S^- sub-populations were increased by up to almost 100-fold in CAMHB-10% (Table S1, see online supplementary material).

As cations are known to interfere with PMB activity by displacing the antibiotic from its binding sites [23], complementary experiments with adjusted Ca^{2+} and Mg^{2+} concentrations were conducted; these showed wide variability between the strains. No effect of cation compensation was observed for ATCC 19606. For AB121-D0, cation compensation tended to suppress the medium dilution effect, with important variability between experiments. Finally, for AB122-D12, cation compensation attenuated the medium dilution effect, indicating that cation dilution explains only part of the increase in kill rate with CAMHB dilution (Fig. 4). However, other cations (Mn^{2+}, Zn^{2+}, etc.) could bind to lipid A and contribute to the medium dilution effect. An effect of Fe^{2+} seems less likely, as the effect of changing Fe^{2+} concentrations on *A. baumannii* growth reported previously [33] was not observed in the present study.

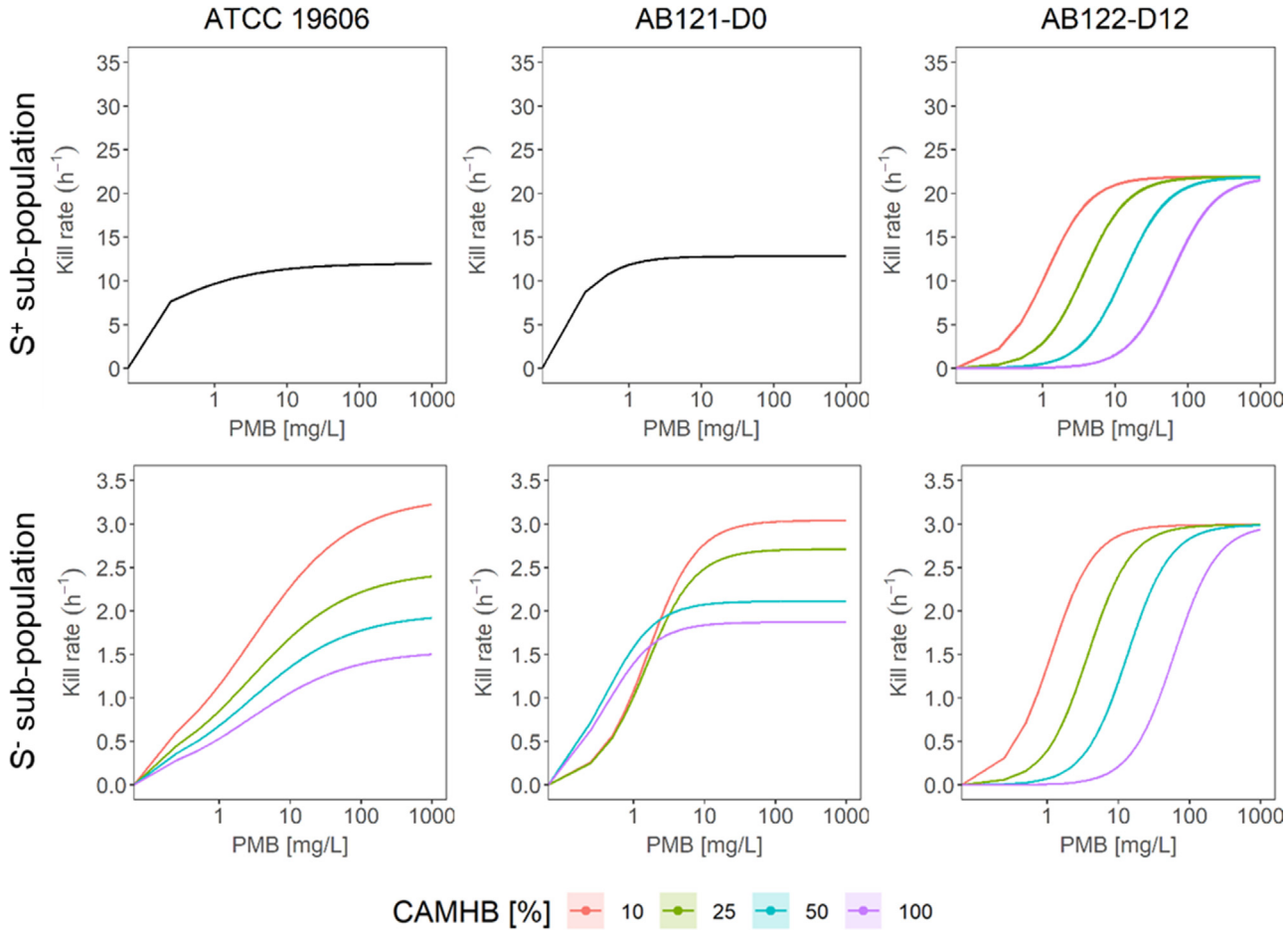

Fig. 3. Simulation of polymyxin B (PMB) kill rate vs. PMB concentrations for various cation-adjusted Mueller-Hinton broth (CAMHB) dilutions. Black lines correspond to kill rate unaffected by CAMHB dilution.

The mechanistic explanation of the medium dilution effect remains unclear, and further studies are needed to understand the impact of the depleted media on bacterial metabolism and/or on compound activity. An increase in the sensitivity of several strains to colistin was observed previously when the pH of the culture medium was alkaline [34]. In the present study, an increase in pH after medium dilution cannot be ruled out, which could have affected the activity of PMB and explain the reduction in apparent bacterial regrowth in this case. The resistant strain AB122-D12 carries a 10 amino acid insertion in pmrB, which is absent in ATCC 19606 and AB121-D0, and known to confer polymyxin resistance through constitutive eptA expression, reducing the overall net-negative charge of the membrane by lipid A modification [35]. If a direct link between mutation and the reinforced medium effect observed for AB122-D12 remains difficult to establish, this cannot be excluded completely as it remains the main difference between the strains. Testing other *A. baumannii* strains with other phenotypes, such as strains carrying mcr-1 plasmid associated with polymyxin resistance, is warranted [35].

The PK/PD modelling approach based on TK experiments allowed differentiation between the impact of dilution on bacterial growth and the antibiotic effect in the presence of initial CFU decay followed by regrowth; this cannot be achieved by traditional PK/PD indices based on MIC. However, the impact of medium dilution on model parameters was described by a discrete function due to the small number of experimental conditions tested, which prevents the extrapolation of model predictions for other dilution factors, and therefore other nutrient and cation concentrations than tested in this study. In addition, major between-strain variability was observed in this study, with no obvious explanation precluding predictions for any other strain, which strongly limits the scope of this work. It should be remembered that the PK/PD model with hetero-resistance used in this study is a mathematical tool to characterize an observed reduction in bacterial sensitivity with time in the presence of an antibiotic, and is probably too simplistic to consider two homogenous sub-populations, with an initial majority of more susceptible bacteria (S^+) leading to the initial CFU decay observed during TK experiments, followed by the development of less susceptible bacteria (S^-) which become dominant over time and responsible for bacterial regrowth. Moreover, although the PD model structure with adaptation was not able to fit the data, it cannot be excluded that adaptation mechanisms could be responsible for bacterial regrowth, as assessed previously with transcriptomics studies [36]. There is a need for more mechanistic information in order to better characterize *in vitro* data.

While *in vitro* experiments allow more experimental freedom to understand biological mechanisms, it is worth considering if the mechanisms will subsequently translate to *in vivo*. First, while the standardized commercial culture media used cannot be directly related to in-vivo environments regarding nutrient composition, this study has shown that the medium has a considerable impact on compound bactericidal activity, even for PMB concentrations that can be found in patients (<10 mg/L [37]). Moreover, in this study, Ca^{2+} and Mg^{2+} compensation was shown to be partially responsible for the medium dilution effect observed, but the compensation was done in order to restore the cation concentrations of the

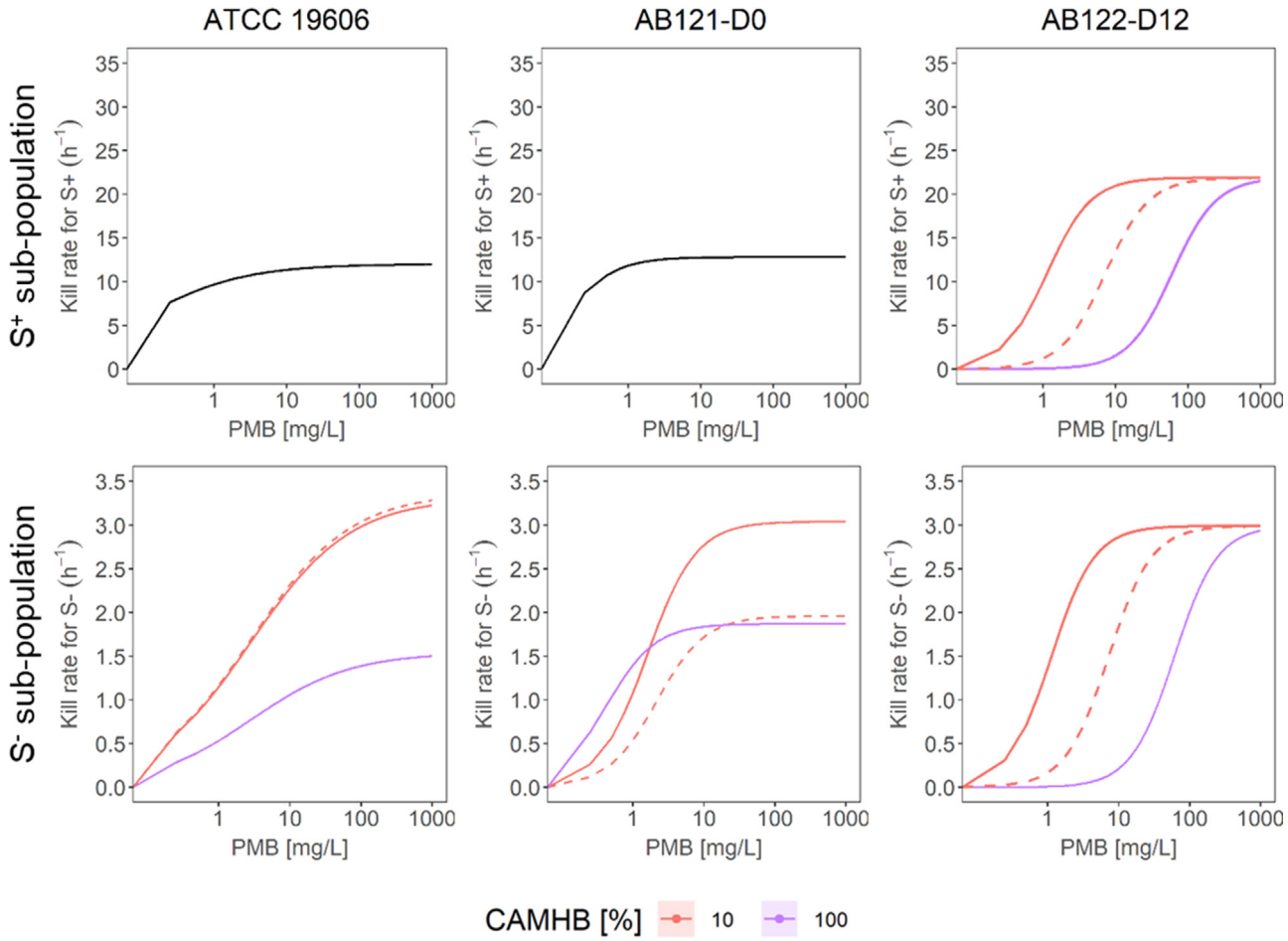

Fig. 4. Simulations of polymyxin B (PMB) kill rate vs. PMB concentrations in cation-adjusted Mueller-Hinton broth (CAMHB)-100% and CAMHB-10% with (dashed lines) and without (solid lines) cation compensation. Black lines correspond to kill rates unaffected by CAMHB dilution.

commercial CAMHB-100%, which remained 2- to 3-fold lower than the concentrations found in plasma or in the extracellular space [38,39]. It is also relevant to highlight that in-vivo results cannot be systematically reproduced during *in vitro* experiments. For example, the mutation of pmrB in AB122-D12 obtained *in vivo* may be observed, but not systematically, during *in vitro* experiments, so AB122-D12 cannot be considered a direct representative of the S^- sub-population of AB121-D0. Furthermore, although relatively popular, the PK/PD model structure used in this study remains a simplification of biological reality, and the significance given to bacterial sub-populations as well as the interpretation of modelling results must be made with caution. In addition, the static TK experiments carried out in more or less rich culture media constitute a first step, and should be completed by dynamic HFIM experiments conducted over a longer period [40], possibly in conditions closer to the environment at the infection site, allowing, for example, biofilm formation [10].

The results of this study indicate that, to some extent, it is possible to adjust the *in vitro* medium to better capture in-vivo efficacy, but questions remain, including the reasons for isolate-specific differences in *in vitro*–in-vivo translation. Further studies are warranted.

Acknowledgements

The authors wish to thank Agnès Audurier and Laure Prouvensier for their technical assistance, and Vincent Aranzana-Climent for his advice regarding modelling.

Funding: ML received a CIFRE fellowship, funded, in part, by the National Association for Research and Technology, on behalf of the French Ministry of Higher Education and Research, and, in part, by Institut Roche

Competing interests: None declared.

Ethical approval: Not required.

Supplementary materials

Supplementary material associated with this article can be found, in the online version, at doi:10.1016/j.ijantimicag.2024.107189.

References

[1] Landersdorfer CB, Nation RL. Limitations of antibiotic MIC-based PK–PD metrics: looking back to move forward. Front Pharmacol 2021;12:770518.
[2] Nielsen EI, Friberg LE. Pharmacokinetic–pharmacodynamic modeling of antibacterial drugs. Pharmacol Rev 2013;65:1053–90.
[3] Palmer ME, Andrews LJ, Abbey TC, Dahlquist AE, Wenzler E. The importance of pharmacokinetics and pharmacodynamics in antimicrobial drug development and their influence on the success of agents developed to combat resistant Gram negative pathogens: a review. Front Pharmacol 2022;13:888079.
[4] Katsube T, Yamano Y, Yano Y. Pharmacokinetic–pharmacodynamic modeling and simulation for in vivo bactericidal effect in murine infection model. J Pharm Sci 2008;97:1606–14.
[5] de Araujo BV, Diniz A, Palma EC, Buffé C, Costa TD. PK-PD modeling of β-lactam antibiotics: in vitro or in vivo models? J Antibiot 2011;64:439–46.
[6] Aranzana-Climent V, Hughes D, Cao S, Tomczak M, Urbas M, Zabicka D, et al. Translational in vitro and in vivo PKPD modelling for apramycin against

Gram-negative lung pathogens to facilitate prediction of human efficacious dose in pneumonia. Clin Microbiol Infect 2022;28:1367–74.
[7] Khan DD, Friberg LE, Nielsen EI. A pharmacokinetic-pharmacodynamic (PKPD) model based on in vitro time-kill data predicts the in vivo PK/PD index of colistin. J Antimicrob Chemother 2016;71:1881–4.
[8] Lin Y-W, Zhou QT, Han M-L, Onufrak NJ, Chen K, Wang J, et al. Mechanism-based pharmacokinetic/pharmacodynamic modeling of aerosolized colistin in a mouse lung infection model. Antimicrob Agents Chemother 2018;62:e01965 -17.
[9] Chauzy A, Akrong G, Aranzana-Climent V, Moreau J, Prouvensier L, Mirfendereski H, et al. PKPD modeling of the inoculum effect of Acinetobacter baumannii on polymyxin B in vivo. Front Pharmacol 2022;13:842921.
[10] Broussou DC, Lacroix MZ, Toutain P-L, Woehrlé F, El Garch F, Bousquet-Melou A, et al. Differential activity of the combination of vancomycin and amikacin on planktonic vs. biofilm-growing Staphylococcus aureus bacteria in a Hollow Fiber Infection Model. Front Microbiol 2018;9:572.
[11] Thorsted A. Pharmacometrics to Characterize Innate Immune Response and Antibacterial Treatments Thesis. Uppsala: Acta Universitatis Upsaliensis; 2020.
[12] Huffnagle GB, Dickson RP, Lukacs NW. The respiratory tract microbiome and lung inflammation: a two-way street. Mucosal Immunol 2017;10:299–306.
[13] Eisenreich W, Dandekar T, Heesemann J, Goebel W. Carbon metabolism of intracellular bacterial pathogens and possible links to virulence. Nat Rev Microbiol 2010;8:401–12.
[14] Son MS, Matthews WJ, Kang Y, Nguyen DT, Hoang TT. In vivo evidence of Pseudomonas aeruginosa nutrient acquisition and pathogenesis in the lungs of cystic fibrosis patients. Infect Immun 2007;75:5313–24.
[15] Veening JG, Barendregt HP. The regulation of brain states by neuroactive substances distributed via the cerebrospinal fluid: a review. Cerebrospinal Fluid Res 2010;7:1.
[16] Flores-Mireles AL, Walker JN, Caparon M, Hultgren SJ. Urinary tract infections: epidemiology, mechanisms of infection and treatment options. Nat Rev Microbiol 2015;13:269–84.
[17] Schwameis R, Fille M, Manafi M, Zeitlinger M, Sauermann R. Enhanced activity of linezolid against Staphylococcus aureus in cerebrospinal fluid. Res Microbiol 2012;163:157–60.
[18] Kussmann M, Hauer S, Pichler P, Reznicek G, Burgmann H, Poeppl W, et al. Influence of different peritoneal dialysis fluids on the in vitro activity of fosfomycin against Escherichia coli, Staphylococcus aureus, Staphylococcus epidermidis, and Pseudomonas aeruginosa. Eur J Clin Microbiol Infect Dis 2018;37:1091–8.
[19] Friberg LE. Pivotal role of translation in anti-infective development. Clin Pharmacol Ther 2021;109:856–66.
[20] Clinical and Laboratory Standards Institute. Performance Standards for Antimicrobial Susceptibility Testing. 33rd Edition. M100. Berwyn, PA: CLSI; n.d. Available at: https://clsi.org/standards/products/microbiology/documents/m100/[accessed 7 March 2023].
[21] European Committee on Antimicrobial Susceptibility Testing. SOP 10.2 MIC distributions and the setting of epidemiological cut- off (ECOFF) values. Available at: https://www.eucast.org/fileadmin/src/media/PDFs/EUCAST_files/EUCAST_SOPs/2021/EUCAST_SOP_10.2_MIC_distributions_and_epidemiological_cut-off_value__ECOFF__setting_20211202.pdf [accessed 7 March 2023].
[22] Mouton JW. Soup with or without meatballs: impact of nutritional factors on the MIC, kill-rates and growth-rates. Eur J Pharm Sci 2018;125:23–7.
[23] Moore RA, Bates NC, Hancock RE. Interaction of polycationic antibiotics with Pseudomonas aeruginosa lipopolysaccharide and lipid A studied by using dansyl-polymyxin. Antimicrob Agents Chemother 1986;29:496–500.
[24] Jaidane N, Naas T, Mansour W, Radhia BB, Jerbi S, Boujaafar N, et al. Genomic analysis of in vivo acquired resistance to colistin and rifampicin in Acinetobacter baumannii. Int J Antimicrob Agents 2018;51:266–9.
[25] Akrong G, Chauzy A, Aranzana-Climent V, Lacroix M, Deroche L, Prouvensier L, et al. A new pharmacokinetic–pharmacodynamic model to characterize the inoculum effect of Acinetobacter baumannii on polymyxin B in vitro. Antimicrob Agents Chemother 2022;66:e0178921.
[26] Tam VH, Schilling AN, Vo G, Kabbara S, Kwa AL, Wiederhold NP, et al. Pharmacodynamics of polymyxin B against Pseudomonas aeruginosa. Antimicrob Agents Chemother 2005;49:3624–30.
[27] Sigma-Aldrich. Mueller Hinton broth 2, cation-adjusted. Sigma-Aldrich; 2018. Available at: https://www.sigmaaldrich.com/deepweb/assets/sigmaaldrich/product/documents/312/461/90922dat.pdf [accessed 19 January 2023].
[28] Beal SL. Ways to fit a PK model with some data below the quantification limit. J Pharmacokinet Pharmacodyn 2001;28:481–504.
[29] Orwa JA, Govaerts C, Gevers K, Roets E, Van Schepdael A, Hoogmartens J. Study of the stability of polymyxins B(1), E(1) and E(2) in aqueous solution using liquid chromatography and mass spectrometry. J Pharm Biomed Anal 2002;29:203–12.
[30] Mouton JW, Vinks AA, Punt NC. Pharmacokinetic–pharmacodynamic modeling of activity of ceftazidime during continuous and intermittent infusion. Antimicrob Agents Chemother 1997;41:733–8.
[31] Dosne A-G, Bergstrand M, Harling K, Karlsson MO. Improving the estimation of parameter uncertainty distributions in nonlinear mixed effects models using sampling importance resampling. J Pharmacokinet Pharmacodyn 2016;43:583–96.
[32] Guo B, Abdelraouf K, Ledesma KR, Chang K-T, Nikolaou M, Tam VH. Quantitative impact of neutrophils on bacterial clearance in a murine pneumonia model. Antimicrob Agents Chemother 2011;55:4601–5.
[33] Eales BM, Bai B, Merlau PR, Tam VH. Growth of Acinetobacter baumannii impacted by iron chelation. Lett Appl Microbiol 2023;76:ovad019.
[34] Panta PR, Doerrler WT. A link between pH homeostasis and colistin resistance in bacteria. Sci Rep 2021;11:13230.
[35] Janssen AB, Schaik W van. Harder, better, faster, stronger: colistin resistance mechanisms in Escherichia coli. PLoS Genet 2021;17:e1009262.
[36] Li M, Aye SM, Ahmed MU, Han ML, Li C, Song J, et al. Pan-transcriptomic analysis identified common differentially expressed genes of Acinetobacter baumannii in response to polymyxin treatments. Mol Omics 2020;16:327–38.
[37] Sandri AM, Landersdorfer CB, Jacob J, Boniatti MM, Dalarosa MG, Falci DR, et al. Population pharmacokinetics of intravenous polymyxin B in critically ill patients: implications for selection of dosage regimens. Clin Infect Dis 2013;57:524–31.
[38] Atchison DK, Beierwaltes WH. The influence of extracellular and intracellular calcium on the secretion of renin. Pflugers Arch 2013;465:59–69.
[39] Romani AMP. Intracellular magnesium homeostasis. Magnesium in the Central Nervous System. Vink R, Nechifor M, editors. Adelaide: University of Adelaide Press; 2011.
[40] Cheah S-E, Li J, Tsuji BT, Forrest A, Bulitta JB, Nation RL. Colistin and polymyxin B dosage regimens against Acinetobacter baumannii: differences in activity and the emergence of resistance. Antimicrob Agents Chemother 2016;60:3921–33.